Biomaterials Science

BMP-2 Delivery Strategy Modulates Local Bone Regeneration and Systemic Immune Responses to Complex Extremity Trauma

Journal:	*Biomaterials Science*
Manuscript ID	BM-ART-10-2020-001728.R1
Article Type:	Paper
Date Submitted by the Author:	22-Dec-2020
Complete List of Authors:	Vantucci, Casey; Georgia Institute of Technology Krishnan, Laxminarayanan; Georgia Institute of Technology Cheng, Albert; Georgia Institute of Technology Prather, Ayanna; Georgia Institute of Technology Roy, Krishnendu; Georgia Tech, Biomedical Engineering Guldberg, Robert; University of Oregon

BMP-2 Delivery Strategy Modulates Local Bone Regeneration and Systemic Immune Responses to Complex Extremity Trauma

Casey E. Vantucci*[1,2], Laxminarayanan Krishan*[2], Albert Cheng[2,3], Ayanna Prather[2], Krishnendu Roy[1,2], Robert E. Guldberg[4]

[1]Wallace H. Coulter Department of Biomedical Engineering, Georgia Institute of Technology and Emory University, Atlanta, GA. [2]Parker H. Petit Institute for Bioengineering and Bioscience, Georgia Institute of Technology, Atlanta, GA. [3]George W. Woodruff School of Mechanical Engineering, Georgia Institute of Technology, Atlanta, GA. [4]Knight Campus for Accelerating Scientific Impact, University of Oregon, Eugene, OR.

Corresponding Author: Robert E. Guldberg, Phil and Penny Knight Campus for Accelerating Scientific Impact, 6231 University of Oregon, Eugene, OR; Phone: 541-346-2120; Email: guldberg@uoregon.edu

Author contributions: *denotes equal contribution. CEV, LK, AC, and AP performed experiments. CEV and LK performed the data analysis. CEV, LK, KR, and REG contributed to data interpretation. LK, KR, and REG designed experiments. CEV wrote the manuscript. CEV, LK, AC, AP, KR, and REG helped make critical revisions to the manuscript. All authors have read and approved the final manuscript.

ABSTRACT

Bone nonunions arising from large bone defects and composite injuries remain compelling challenges for orthopedic surgeons. Biological changes associated with nonunions, such as systemic immune dysregulation, can contribute to an adverse healing environment. Bone morphogenetic protein 2 (BMP-2), an osteoinductive and potentially immunomodulatory growth factor, is a promising strategy; however, burst release from the clinical standard collagen sponge delivery vehicle can result in adverse side effects such as heterotopic ossification (HO) and irregular bone structure, especially when using supraphysiological BMP-2 doses for complex injuries at high risk for nonunion. To address this challenge, biomaterials that strongly bind BMP-2, such as heparin methacrylamide microparticles (HMPs), may be used to limit exposure and spatially constrain proteins within the injury site. Here, we investigate moderately high dose BMP-2 delivered in HMPs within an injectable hydrogel system in two challenging nonunion models exhibiting characteristics of systemic immune dysregulation. The HMP delivery system increased total bone volume and decreased peak HO compared to collagen sponge delivery of the same BMP-2 dose. Multivariate analyses of systemic immune markers showed the collagen sponge group correlated with markers that are hallmarks of systemic immune dysregulation, including immunosuppressive myeloid-derived suppressor cells, whereas the HMP groups were associated with immune effector cells, including T cells, and cytokines linked to robust bone regeneration. Overall, our results demonstrate that HMP delivery of moderately high doses of BMP-2 promotes repair of complex bone nonunion injuries and that local delivery strategies for potent growth factors like BMP-2 may positively affect the systemic immune response to traumatic injury.

1. INTRODUCTION

Five to ten percent of the more than twelve million fractures a year experience complications with healing, most commonly nonunions and infections (1–3). Nonunions can be considered as any fracture that persists without any healing progression for at least 3 months. In rodent models, this can be accomplished by creation of a critical size segmental bone defect which will always lead to non-union (4). For composite injuries, which contain volumetric tissue defects in both the bone and the adjacent soft tissue and muscle, the risk for nonunion is twice as high (3,5). Revision surgery to address nonunions is typically successful in upwards of 90% of patients; however, chronic nonunions that result after one or more failed interventions still pose a significant clinical challenge. Chronic nonunions are defined as a fracture that has failed to heal for more than 12 months, and they can result in multiple revision surgeries, prolonged hospital stays, increased treatment costs, and even limb loss, with one prospective study reporting around 2% of patients undergoing amputations following nonunion of a severe lower limb extremity trauma (3,5). Despite advancements in surgical procedures and regenerative strategies, there is still an urgent need for improved treatment strategies for chronic nonunions (7).

Currently, the exact underlying biological and physiological mechanisms leading to the development of nonunion are poorly understood, and further, how these biological changes impact treatment outcomes for patients is also poorly understood (8). It is generally accepted that there are various risk factors, such as age, gender, smoking, and medical comorbidities, that can increase the likelihood of nonunion and decrease treatment success; however, recent work has also identified other factors that can impact treatment outcomes for trauma patients, including systemic immune function (9). Long-term poor clinical outcomes, such as chronic nonunions, have been

associated with systemic immune dysregulation and immunosuppression, marked by functional decreases in immune effector cells and cytokines and increases in immunosuppressive cells and cytokines (10). Systemic immune dysregulation is hypothesized to occur when the immune system overcompensates for high levels of inflammation, and this has been observed clinically and in pre-clinical models following severe injury, sepsis, and orthopedic infection (11–13). Additionally, observation of systemic immune dysregulation in a pre-clinical model of chronic nonunion revealed correlations between impaired bone healing and systemic cytokine expression (14). The immune system is essential for appropriate and regulated healing, and the field of osteoimmunology has highlighted the complex relationship between bone and the immune system (15). It is unknown if improper functioning of the systemic immune system contributes to nonunion progression or results from nonunion progression; however, treatment strategies that are not only osteogenic but also capable of overcoming systemic immune dysregulation could be essential to improving patient outcomes following treatment of chronic nonunions.

One treatment approach for complex bone injuries employs bone morphogenetic protein 2 (BMP-2) delivered on an absorbable collagen sponge (16–18). BMP-2 is a potent osteoinductive growth factor with FDA approval for use in select applications like spinal fusions and some tibial fractures; however, pre-clinical and clinical studies over the past 10 years have shown significant promise for BMP-2 treatment in long bone fractures (19,20). In addition, BMP-2 has exhibited a positive immunomodulatory effect through macrophage stimulation and upregulation of cytokines important for MSC recruitment and angiogenesis, resulting in enhanced osteogenesis of bone marrow stromal cells (21). Despite clinical use of collagen sponges for BMP-2 delivery, they have been shown to retain only 10% or less of the BMP-2 at the implant site 1 to 2 weeks after delivery,

minimizing treatment efficacy and increasing risk for adverse side effects such as inflammation, heterotopic ossification (HO), and irregular bone organization (22–27). Delivery vehicles with improved spatiotemporal release profiles may be essential for decreasing unwanted side effects and improving efficacy by maintaining BMP-2 locally and preventing systemic spread of BMP-2. In addition, by maintaining BMP-2 locally, these improved delivery vehicles could also allow for safe and controlled delivery of higher BMP-2 doses, which may be beneficial since bone healing has previously exhibited a dose response to BMP-2 (14,22,28). For example, in a rat chronic nonunion bone defect model, treatment with 2.5ug BMP-2 resulted in only a 50% bridging rate of the defect, whereas 5ug BMP-2 resulted in a 75% bridging rate (14). Similarly, in a rat composite bone-muscle defect model, acute treatment with 10ug BMP-2 showed increased bone regeneration compared to a 2.5ug BMP-2 dose (28). Additionally, both studies showed enhanced mechanical properties, including strength and stiffness, at the higher BMP-2 doses. Interestingly, these dosages in the rat correspond to human dosages around 5-10 times below the typical clinical dosage of 0.1-0.5mg/kg. Higher dosages of BMP-2 need to be evaluated to better correspond to clinical practices. In addition, the ability to spatiotemporally deliver even higher doses of BMP-2 may be essential for minimizing side effects and for sustaining endogenous repair mechanisms that could improve outcomes, especially in more challenging bone defect scenarios, such as chronic nonunions.

Many alternatives to collagen sponges have been investigated in pre-clinical models to improve BMP-2 retention and prevent rapid release, including polylactic-co-glycolic acid (PLGA) and alginate (29–31), and these, along with other strategies, have been extensively reviewed (32–34). One particularly promising approach to appropriately deliver high doses of BMP-2 utilizes heparin, a naturally occurring biomolecule, that can retain large amounts of bioactive BMP-2

through reversible, non-covalent electrostatic interactions (35,36). Our laboratory has previously fabricated heparin methacrylamide microparticles (HMPs) loaded with BMP-2 that can easily be incorporated within an alginate hydrogel which is then spatially constrained to the injury site by a polycaprolactone nanofiber mesh (28). This HMP delivery system enhances the spatiotemporal release profile of moderately high doses of BMP-2, increases long-term retention of BMP-2 at the defect site, and decreases heterotopic bone formation in a pre-clinical bone defect model when treated immediately after injury (37–39), all highlighting the potential of this strategy for successful and controlled delivery of high doses of BMP-2. The ability to safely deliver higher doses of BMP-2 through the HMP system may allow BMP-2 to act as both an osteoinductive and immunomodulatory agent to overcome additional immunological challenges associated with chronic nonunions, ultimately enhancing bone regeneration. At the same time, excessive doses of BMP-2 could harmful, so appropriate dosing for the type and severity of trauma is essential.

In this study, a moderately high dose of BMP-2 (30ug or 0.12mg/kg) delivered from clinical standard collagen sponge is compared to the same dose of BMP-2 delivered from our previously established HMP delivery system in two clinically-relevant chronic nonunion models: a bone defect chronic nonunion model and a more severe composite injury chronic nonunion model with concomitant volumetric muscle loss. While this strategy showed promise in an acutely treated segmental defect model, this is the first time that this delivery strategy has been investigated in more complex and challenging chronic nonunion models exhibiting systemic immune dysregulation, which has previously been associated with poor patient outcomes. Specifically, two main hypotheses are investigated: first, that the high dose BMP-2 delivered through the HMP system will promote spatially controlled functional bone regeneration in chronic nonunion models,

even under challenging conditions exemplified by the composite bone-muscle injury model; and second, that spatially controlled BMP-2 release from the HMP system will support immunomodulatory functions of BMP-2 that result in positive modulation of the systemic immune response. A better understanding of the regenerative response to therapeutic strategies and the immunological changes and biological mechanisms associated with nonunion progression are both critical to improving patient outcomes and reducing the morbidity associated with challenging bone nonunions.

2. MATERIALS AND METHODS

2.1 Delivery vehicle preparation

2.1.1 Heparin Microparticle Fabrication

Heparin microparticles were fabricated as previously described (37,38). Briefly, EDC/Sulfo-NHS chemistry was used to substitute methacrylamide groups on heparin. Heparin methacrylamide was then dissolved in phosphate-buffered saline (PBS) and mixed with equimolar amounts of the free radical initiators, ammonium persulfate (Sigma Aldrich) and tetramethylethylenediamine (TEMED, Sigma Aldrich). A water-in-oil emulsion was then formed by adding the heparin solution dropwise into 60mL of corn oil and 1mL of polysorbate 20 (Promega) and then homogenized on ice for 5 min at 3000rpm (Polytron PT3100 Homogenizer, Kinematica). Free radical polymerization and thermal cross-linking of the methacrylamide groups was carried out by immersing the emulsion in a 55˚C water bath under constant stirring and nitrogen purging for 30 minutes. The HMPs were collected following centrifugation for 10 minutes at 3000rpm and subsequently washed in acetone, deionized water several times, and 70% ethanol for sterilization. HMPs were lyophilized and stored at 4˚C until ready for incorporation into the alginate constructs.

HMPs were characterized following fabrication and confirmed to retain their functionality with evaluation of growth factor binding and release kinetics (38).

2.1.2 Alginate and Nanofiber Mesh Construct Fabrication

Alginate hydrogels were fabricated as previously described (31). Briefly, a 3% alginate solution was made by slowly dissolving irradiated, RGD-functionalized alginate (FMC Biopolymer) into sterile alpha-MEM (Corning). The solution was then mixed with 0.1% rat serum albumin (RSA) in 4mM HCl containing 30ug of BMP-2 and 0.1mg of HMPs to make a 2% alginate solution. The final alginate solution containing BMP-2 and HMPs was then cross-linked in an excess of calcium sulfate (8.4mg/mL; Sigma Aldrich) by thorough mixing and stored in 4˚C. Polycaprolactone (PCL) nanofiber meshes were fabricated as previously described (31). Briefly, a 12% (w/v) PCL solution is formed by dissolving PCL overnight in a 90:10 solution of 1,1,1,3,3,3-Hexafluoro-2-propanol, 99+% (HFP; Sigma Aldrich) and *N,N*-Dimethylformamide, anhydrous, 99.8% (DMF; Sigma Aldrich). The PCL solution is then electrospun onto aluminum foil until an approximate thickness of 500um. Rectangular perforated meshes (12mm by 19mm with 0.7mm diameter holes) were then cut from the electrospun PCL nanofiber meshes and rolled to have an inner diameter of 4.5mm and a length of 12mm. The meshes were glued with UV cure adhesive (DYMAX), sterilized in 70% ethanol, and then stored in alpha-MEM at 4˚C until use. For *in vivo* studies, the PCL nanofiber mesh tube was placed within the defect site and subsequently 150uL of the alginate hydrogel was syringe injected with a blunt-tip needle into the center of the mesh so each defect received 0.1mg HMPs and 30ug BMP-2.

2.2 Surgical procedures

All animal procedures were performed in accordance with the Guidelines for Care and Use of Laboratory Animals of the Georgia Institute of Technology and approved by the Animal Ethics

Committee of the Georgia Institute of Technology. Thirteen-week old female Sprague Dawley rats (Charles River Laboratories) received a unilateral segmental defect in the left femora, as previously described (40). Briefly, a polysulfone internal fixation plate provided stabilization while an oscillating saw was used to remove 8mm from the mid-diaphysis of the femur. The polysulfone plate sits outside the defect region on metal risers that are about 2-3mm thick. In the composite defect animals, an additional 8mm diameter, full-thickness defect was created in the overlying quadriceps, as previously described (41). All defects were left untreated until 8 weeks post-surgery. At 8 weeks, animals underwent an additional procedure where the defect site was cleared, and treatment was administered (Figure 1A). Animals received a clinically-equivalent dose of 30ug BMP-2 (0.12kg/mg) loaded in a collagen sponge, n=10 (DSM) or in the HMP delivery system (HMPs in alginate gel + PCL nanofiber mesh), n=11 (Figure 1B). Additionally, all composite defect animals received 30ug BMP-2 delivered in the HMP system, n=6, and the muscle defects were left untreated. In order to minimize animal number used, there was no collagen sponge treated composite defect group since previous work in our lab has consistently shown that composite defects heal worse compared to bone only defects with the same treatment (41). Therefore, comparisons between the HMP treated composite defect group and the collagen sponge treated bone defect only group exhibit treatment outcomes despite the additional challenge of a muscle defect. Following surgical procedures, animals were given ad libitum access to food and water and showed no signs of pain or distress. Animals were euthanized by CO_2 inhalation at twenty weeks from the first surgical procedure.

2.3 Bone regeneration

2.3.1 Radiography and micro-computed tomography

Longitudinal bone regeneration was qualitatively assessed with radiographs taken at 4, 8, and 12 weeks post-treatment (12, 16, and 20 weeks post-injury) (Faxitron MX-20 Digital, Faxitron X-ray Corp.). At the same time points, micro-computed tomography (Viva-CT 40, Scanco Medical) was used for quantitative assessment of newly regenerated bone, determined using a threshold corresponding to ≥ 50% of the density of native cortical bone. Along the long axis of the femur, the central 166 slices (~6.5mm of the 8mm defect) were evaluated with a 38um voxel size, 55kVp voltage, and 145uA current. To differentiate between bone formed within the defect (defect bone volume) and bone formed outside of the defect (heterotopic bone volume), 2 volumes of interest (VOI) were evaluated, as previously described (17). The first VOI encompassed a large diameter to characterize all bone formation within the thigh, while the second VOI encompassed only a 6mm-diameter to characterize bone formation within and immediately bordering the PCL nanofiber mesh. Heterotopic bone volume was determined by subtracting the bone volume of the second VOI (defect bone volume) from the bone volume of the first VOI (total bone volume) (Figure 4A). Trabecular thickness, trabecular number, and connectivity were determined using a Scanco evaluation script according to previously set guidelines for assessing bone microstructure in rodents (42). Polar moment of inertia (pMOI) was also determined using a Scanco evaluation script that measures and calculates the bone distribution along the central longitudinal axis for each individual slice. These values are then averaged to determine a global pMOI value for each sample (17,43).

2.3.2 *Biomechanical testing*

Following euthanasia at the week 20 endpoint, femora were harvested for biomechanical testing. The soft tissue was cleared, and the fixation plates were carefully removed. Each femur end was then potted in Wood's metal (Alfa Aesar) and tested to failure in torsion at a rotation rate of 3˚ per

second (ELF 3200, TA ElectroForce), as previously described (40). Torque-rotation curves were used to calculate failure strength (maximum torque) and torsional stiffness for each sample. Contralateral femora were used to determine biomechanics of intact bone.

2.3.3 *Histological analysis*

After mechanical testing, one representative sample from each group was selected for histology. The samples were fixed in 10% neutral buffered formalin (NBF) for 24 hours and then decalcified in a formic citrate solution (Newcomer Supply, Inc). The bone tissue was embedded in paraffin and sectioned at a thickness of 5 um and then stained with hematoxylin & eosin (H&E) and safranin-O/fast green (Histotox Labs; Boulder, CO).

2.4 Immune characterization

Approximately 500uL of blood was collected longitudinally via the rat tail vein at weeks 0 (baseline), 2, 8 (prior to treatment), 10, and 20. Half of the blood collected was allowed to clot overnight at 4˚C. The next day, the samples were centrifuged down at 1500g for 10 minutes and the serum was collected and stored at -20˚C for cytokine and chemokine analysis. The other half of the blood collected was stored in heparin coated tubes to prevent clotting. Following red blood cell lysis (1X RBC Lysis Buffer, eBioscience,), cells were fixed (BD Cytofix, BD), resuspended in FACS buffer (2% fetal bovine serum in 1X PBS), and then stored at 4˚C until staining for cellular analysis via flow cytometry.

2.4.1 Cellular analysis

Flow cytometry was used to evaluate circulating immune cell populations. Prior to staining, cells were blocked with anti-rat CD32 (BD) for 10 minutes at 4˚C to prevent non-specific binding. Samples were then stained for the following immune effector cell populations: T cells (CD3+), helper T cells (CD3+CD4+FoxP3-), cytotoxic T cells (CD3+CD8+), and B cells (B220+). Samples

were also stained for the following immunosuppressive cell populations: myeloid-derived suppressor cells (MDSCs, His48+CD11b+) and T regulatory cells (Tregs, CD3+CD4+FoxP3+). All antibodies were purchased from eBioscience. Data were collected using a BD Accuri C6 flow cytometer, and FlowJo was used for data analysis. All gates were set based on fluorescent minus one (FMO) and unstained controls with less than 1% noise allowed.

2.4.2 Cytokine and chemokine analysis

Serum cytokines and chemokines were evaluated via a multiplexed immunoassay (Milliplex MAP Rat Cytokine/Chemokine Magnetic Kit, Millipore Sigma), and data were collected using a MAGPIX Luminex reader (Luminex). Median fluorescent intensity values with the background subtracted were used for multivariate analyses.

2.5 Statistical analysis and partial least squares discriminant analysis

Cytokine, chemokine, and cellular data were compiled at each time point for multivariate analysis using partial least squares discriminant analysis (PLS-DA). PLS-DA analysis reduces the dimensionality of the input variables into a set of latent variables (LVs) that maximally separate discrete groups (i.e. collagen sponge treatment group vs. HMP treatment groups). Latent variables are composed of profiles of the input variables that represent their relative contributions to the latent variables, and thus the separation between the groups. PLS-DA was conducted in MATLAB (Mathworks) using Cleiton Nunes' partial least squares algorithm (Mathworks File Exchange) following z-scoring to normalize the data. All data are represented as the mean ± standard deviation, and analyses were conducted using GraphPad Prism 7. Parametric and non-parametric statistical tests were used as indicated based on if assumptions were met or not.

3. RESULTS

3.1 Clinically-relevant bone nonunion models

Two previously established and challenging animal models of chronic nonunion were used in this study: one consisting of a segmental bone defect (Bone Only) and the other consisting of a segmental bone defect with concomitant volumetric muscle loss (Composite), representing a more challenging case of nonunion. In both models, treatment was delayed until 8 weeks after creation of the defect at which point capping of the bone ends was seen, indicating little or no further mineralization and establishment of nonunion. Following treatment with 30ug BMP-2 delivered in either the HMP construct or the clinical standard collagen sponge (Figure 1B), animals underwent longitudinal evaluation of bone regeneration and the systemic immune response for an additional 12 weeks (week 20 after the initial defect surgery; Figure 1C). At Week 0 prior to treatment (8 weeks post-injury), circulating immune cell populations were evaluated and compared to baseline levels that had been assessed immediately prior to injury. T cells were significantly decreased compared to baseline levels, whereas immunosuppressive MDSCs and macrophages were significantly elevated in both the Bone Only and Composite injury groups (Figure 2). Although there was no significant difference in B cell populations, B cells did show a decreased peak in cell counts compared to baseline (Figure 2).

3.2 Radiography and micro-computed tomography

Radiographs demonstrated qualitative bridging in all samples regardless of group; however, they also revealed larger variability in healing responses in the collagen sponge group compared to the HMP treated groups (Figure 3A). In order to minimize animal number used, a collagen sponge treated composite defect group was not included since previous work in our lab has consistently shown that composite defects heal worse compared to bone only defects with the same treatment (41). Therefore, comparisons between the HMP treated composite defect group and the

collagen sponge treated bone defect only group exhibit treatment outcomes despite the additional challenge of a muscle defect. Representative samples with low and high amounts of heterotopic ossification (HO) in each group showed that the collagen sponge group had increased HO compared to the HMP groups. Additionally, the collagen sponge group also had a lower valley of HO compared to the HMP groups, although this appears to be due to decreased overall bone volume. In contrast, samples in the HMP groups with the highest and lowest levels of HO appeared much more consistent and similar with robust defect bone formation and minimal heterotopic bone formation, although the more challenging composite nonunion model appeared to have slightly more HO than the bone only nonunion model. The radiographs are supported by uCT reconstructions, again showing increased variability and higher peak HO in the collagen sponge group compared to the HMP groups (Figure 3B).

Quantitation of uCT reconstructions additionally supports radiographic observations. The HMP delivery strategy resulted in significantly increased new total bone volume at both 4 and 8 weeks post-treatment in both nonunion models (Figure 4B). Looking more specifically at bone formed within the defect site, there were clear differences between the BMP-2 delivery strategies. Similar to total bone volume, the HMP groups had significantly increased defect bone volume at both 4- and 8-weeks post-treatment (Figure 4C). Although there were no significant differences in heterotopic bone volume, at 12 weeks post-treatment, the HMP groups exhibited decreased variability of HO at week 8 (Brown-Forsythe test, $p=0.07$) and at week 12 (Brown-Forsythe test, $p=0.09$) and a lower level of peak HO at week 12 compared to the collagen sponge group (Figure 4D). The percentage of heterotopic bone observed in each group also shows lower peak HO in the HMP groups compared to the collagen group. Further, at week 12, 40% of the collagen group exhibited higher HO compared to any sample in either of the HMP groups, and 70% of the collagen

group exhibited higher HO than the average HO in both of the HMP groups (Figure 4E). Because irregular bone formation can be an adverse side effect of BMP-2 administration, we also investigated the trabecular number, trabecular thickness, and connectivity of the newly formed bone. Here, the HMP group for the bone only nonunion model had significantly increased trabecular number at all weeks post-treatment compared to the collagen sponge group (Figure 4F). Both HMP groups exhibited significantly increased trabecular thickness and connectivity at weeks 8 and 12 post-treatment compared to the collagen sponge group (Figure 4G,H). There were no significant differences in the polar moment of inertia between groups (Figure 4I).

3.3 Biomechanical testing and histological analysis

Endpoint evaluations of bone regeneration included both biomechanical testing and histological analysis. There were no significant differences between groups in the torque to failure; however, all groups exhibited lower failure strengths compared to intact bone (Figure 5A). Further, there were no differences in torsional stiffness between groups, and all were slightly higher than the stiffness of intact bone (Figure 5B). Prior finite element modeling at sub-failure rotation demonstrates that the largest strains are present in the outermost connected regions and there is minimal strain along the central access (17). Therefore, the central bone actually contributes relatively little to the mechanical properties measured by torsion testing.

Qualitative histological analysis of bone regeneration (Figure 5C) supports both the radiographs and the quantitative uCT data. Hematoxylin & Eosin and Safranin-O/Fast Green staining both reveal larger sections of mineralized tissue in the HMP groups. In the collagen sponge group, there are larger areas of non-mineralized, marrow-like tissue compared to the HMP groups; although, the composite nonunion HMP-treated group did have larger areas of marrow-like tissue compared to the bone only nonunion HMP-treated group. Residual alginate can also be seen in

the HMP groups, indicating that the tissue engineered construct remained within the defect site. More fatty infiltrate into the marrow cavity can be seen within the composite defect group compared to the segmental defect only groups.

3.4 Systemic immune characterization

Blood was collected at the baseline (prior to injury) and at various timepoints following injury and treatment in order to assess the systemic immune response. While there were changes in circulating immune cell populations over time, there were no differences in immune cell populations between treatment groups at any time point (Supplementary Figure 1). Additionally, there were no differences in cytokine levels across treatment groups at any time point (Supplementary Figure 2).

We hypothesized that the lack of differences for markers of the systemic immune response between the HMP-treated and collagen sponge groups could be due to the wide variability of responses in the collagen sponge group. Therefore, to better understand the relationship between the systemic immune response and healing, linear regression of immune cell populations at the Week 12 endpoint for all samples together was performed against defect bone volume (as a percent of the total bone volume). Defect bone volume was selected as a metric for good healing because it encompassed animals with high defect bone volume in addition to low heterotopic bone formation. Linear regression of week 12 MDSCs versus defect bone volume percent showed a significant negative correlation (Figure 6A, $r^2 = 0.24$, $p = 0.012$), whereas linear regression of week 12 CD3+ T cells and week 12 effector T cells (CD3+CD4+ cells and CD3+CD8+ cells) versus defect bone volume percent both showed positive correlations (Figure 6B and Figure 6C). In an effort to better understand the best and worst responders, we compared the top and bottom quartiles of defect bone volume data and compared differences in immune cell populations. The top quartile

of responders (best responders) consisted of 4 out of 7 from the HMP-treated groups, and the bottom quartile of responders (worst responders) consisted of 6 out of 7 from the collage sponge group. Comparisons between the best and worst responders revealed more pronounced differences in immune cell populations with the top quartile of responders exhibiting lower numbers of MDSCs ($p = 0.011$, Figure 6D), higher numbers of CD3+ cells ($p = 0.13$, Figure 6E), and higher numbers of effector T cells ($p = 0.098$, Figure 6F) compared with the bottom quartile of responders.

These analyses highlight that the complexities of the immune response, especially for average responders, which may mask differences between individual cells and cytokines. Hence, multivariate partial least squares discriminant analysis (PLS-DA) was performed to better determine further differences in the overall systemic immune response between groups. Immune cell and cytokine levels at all timepoints were compiled for PLS-DA. Results show no separation of data between the HMP and collagen sponge groups based on the latent variable 1 (LV1) axis (Figure 7A). However, there is separation along the latent variable 2 (LV2) axis with the HMP groups having significantly lower LV2 scores compared to the collagen sponge group (Figure 7B). The LV2 loading plot reveals the immune factors that most contribute to the higher and lower LV2 scores, showing which cells and cytokines are most correlated with the collagen sponge treated group versus the HMP treated groups (Figure 7C). The top factors most associated with the HMP groups were T cells, including the helper (CD4+) and cytotoxic (CD8+) T cell subsets, and the hormone leptin. On the other hand, the top factors most associated with the collagen sponge group include the immunosuppressive MDSCs and Tregs as well as the chemotactic factors LIX and RANTES, also known as CXCL5 and CCL5, respectively.

4. DISCUSSION

Despite advances in trauma care management, orthopedic surgeons still need better strategies to improve outcomes for patients with chronic nonunions, especially for more challenging cases with concomitant volumetric muscle loss. While there are many factors that influence nonunions and bone healing, one promising strategy has focused on the delivery of BMP-2 in an absorbable collagen sponge. However, if not contained to the injury site, BMP-2 has been shown to have adverse side effects, highlighting the need for improved delivery vehicles that can maintain BMP-2 bioavailability and minimize side effects. Previously, our lab evaluated an HMP hybrid delivery system in an acutely treated segmental defect model, which resulted in increased long-term retention of BMP-2 at the defect site and decreased heterotopic bone formation (37–39). The current study evaluates delivery of a moderately high dose (30ug) of BMP-2 from this same HMP delivery system in two more complex and challenging chronic nonunion models, and additionally, this study attempts to preliminarily evaluate the systemic immunological changes associated with each delivery system.

Evaluation of circulating immune cell populations show changes in the immune response over time prior to treatment of the defect when compared to pre-injury baseline levels, with significant decreases in T cells and increases in immunosuppressive MDSCs and macrophages (Figure 2). These changes are characteristics of systemic immune dysregulation observed clinically in trauma patients and have been associated with increased susceptibility to infection and decreased treatment success (44–47). Following severe trauma, damaged tissue and high levels of inflammation lead to a systemic inflammatory response, marked by increases in pro-inflammatory mediators and activation of innate immune cells (48–50). To prevent against harmful levels of systemic inflammation, a compensatory anti-inflammatory immune response develops to

counteract the initial inflammation and restore immune homeostasis, marked by increases in anti-inflammatory cytokines and increases in immunosuppressive cells, such as MDSCs and Tregs (38,39). However, in some patients, especially those with complications and more challenging injuries, the compensatory anti-inflammatory response overcompensates for the initial inflammation and immune homeostasis is not restored, resulting in systemic immune dysregulation and immunosuppression (51). Systemic immune dysregulation has been associated with decreased success of treatment; and therefore, effective treatment strategies may need to be able to overcome any adverse immunological changes that could hinder successful healing. Our chronic nonunion model exhibits characteristics of systemic immune dysregulation and could therefore allow for new regenerative strategies to be evaluated in a more clinically-relevant model by more accurately representing the immune environment at the time of treatment. This more recent interest in the systemic immune response differs from historical data that has typically associated local immune responses with interventional outcomes. However, systemic immune markers may offer more promise than local immune data because systemic immune markers can be used clinically to identify patients at-risk for poor healing. This information would be easy to obtain non-invasively and longitudinally in a clinical setting through routine blood draws. In comparison, local immune data is not easy to obtain in a clinical setting. For these reasons, we chose to more heavily investigate the systemic immune response in this study. Further work will aim to evaluate not just the population levels of circulating immune cells, but also their function. Additionally, while our model did not include a naïve group to confirm that the immunological changes observed are not simply due to aging, the 8-week delayed treatment time period is still well within what is considered a young adult rat (53). Typically, immunoaging and immunosenescence begin past

adulthood, so there should not be significant immunological changes occurring in our model due to aging over the time course of this study (54,55).

We observed differences in bone regeneration between the two delivery vehicles for high-doses of BMP-2, with the HMP delivery system resulting in more consistent and robust bone regeneration compared to the collagen sponge delivery vehicle, even despite the additional challenges historically associated with chronic nonunions and concomitant muscle injury. The most significant challenge BMP-2 usage faces clinically is the adverse side effects, including excessive inflammation, heterotopic ossification and irregular bone formation, which can lead to pain and less desirable patient outcomes (24–27). The HMP delivery system showed increased bone formation within the defect, lower peak heterotopic ossification, lower percentage of heterotopic bone, and more regular bone formation compared to the collagen sponge delivery group. Decreased side effects can be attributed to increased bioavailability and retention of the BMP-2 at the injury site. Bone formation can be attributed to the system's ability to appropriately retain and slowly release BMP-2, even though the biomaterials themselves likely have minimal impact on bone formation. The nanofiber mesh and alginate hydrogel alone have been shown to result in minimal bone formation in previous studies (17,31). In addition, we have also previously investigated delivery of BMP-2 in the alginate/mesh system alone or on HMPs within the alginate/mesh system and have seen significant differences in bone formation, highlighting the specific role of HMPs on bone formation (56). BMP-2 alone would not be expected to enhance bone formation because BMP-2 would diffuse out of the defect region rapidly, resulting in more heterotopic bone formation and negative systemic side effects. Although the biomaterial itself may

have minimal direct impact on bone formation, it enables specific spatiotemporal delivery of BMP-2 that directly results in the bone formation patterns observed.

Heparin is one of the key components to the hybrid delivery system and is a glycosaminoglycan (GAG). GAGs are molecules that make up components of the extracellular matrix (ECM) and are naturally involved in binding and sequestering growth factors in the cellular microenvironment (57,58). The strong negative charge allows for a high affinity and reversible electrostatic interaction with BMP-2 which increases retention within the alginate gel and at the injury site, stimulating progenitor cells and endogenous repair mechanisms (38,59,60). Although heparin is a known anti-coagulant and has been shown to inhibit angiogenesis (61), delivery of a potent angiogenic factor (BMP-2) likely outweighs any potential effects of heparin on angiogenesis, which is essential during the bone regeneration process. In vitro evaluation of BMP-2 release from HMPs showed sustained release over a 4 week period, with low burst release (<10% in the first 6 hours). The cumulative percentage of BMP-2 released over the 4 week period was independent of loading mass and was <20% of the loaded BMP-2, demonstrating the capability of the HMPs to retain BMP-2. The presence of the alginate tissue engineered construct can be observed in histological stain 12 weeks after treatment within the defect site, although it is unknown how much BMP-2 remains in the construct. The uncontrolled burst release of BMP-2 from the collagen sponge delivery system decreases bioavailability (23), leading to decreased bone formation within the defect and increased side effects, including higher percentage of heterotopic ossification, higher peak HO and irregular bone formation. Additionally, the inconsistent and uncontrolled release of BMP-2 from collagen sponge leads to similarly inconsistent bone healing results with wide variability in response to treatment, which is undesirable for clinical applications. Differences

in bone formation can also be observed in the histology images with increased bone formation in the HMP groups. Interestingly, there is more lipid and fatty infiltration in the composite defect group, which has been observed previously in skeletal muscle trauma especially for larger volumetric defects (62). Bone marrow adipose tissue has previously been shown to decrease bone regeneration (63), which could be a contributing mechanistic factor to differences in bone regeneration in the composite group versus the bone only group. Despite clear differences between the two delivery groups from radiographs, uCT, and histology, there were no significant differences in the biomechanics of the newly formed bone between the two groups. However, the method of mechanical testing evaluates the strength and stiffness is biased towards the outermost regions of bone, not defect bone formation, meaning the higher percentages of heterotopic ossification observed in the collagen sponge delivery group likely inflated the observed mechanical properties. This lack of difference in mechanical properties aligns with the uCT polar moment of inertia data (Figure 4I) which shows no significant differences in the spatial extent of bone formation. However, despite the lack of biomechanical differences, the HMP delivery system still had improved spatial localization of bone regeneration compared to the collagen sponge for two challenging cases of nonunion with adverse systemic immune environments.

Along with optimizing spatiotemporal BMP-2 delivery with appropriate scaffolds, the immunological host response to severe injury presents additional challenges for successful treatment. Although there were no differences between the groups for individual cell populations or cytokines by routine univariate comparisons between groups, this may be due to the complexities of the immune system and extensive interactions between immune mediators (64). The pleiotropic and redundant interactions between various cytokines and cells make it difficult to

identify clear differences between immune responses without the help of multivariate analyses that can minimize effects of confounding factors and reduce noise. Following multivariate analyses, the cell populations most associated with the collagen sponge group include the immunosuppressive MDSC and Treg populations. Notably, these are the cell populations that most contribute to systemic immune dysregulation, with MDSCs increased prior to treatment. The continued association with these cell types suggests that the collagen sponge group may not have been successful at overcoming the additional challenge associated with immune dysregulation. On the other hand, the cell types most associated with the HMP groups include all CD3+ T cells, including the CD4+ helper and CD8+ cytotoxic T cell subsets. Increased numbers and function of immune effector cells are essential for restoration of immune homeostasis and re-establishment of a pro-healing and pro-regenerative immune environment, suggesting that the HMP groups were more successful at addressing the systemic immune dysregulation present at the time of treatment based on multivariate discriminant analyses. The cytokines most associated with the collagen sponge group included LIX and RANTES, also known as CXCL5 and CCL5. LIX is released from inflammatory and endothelial cells and is known for its chemotactic and activation properties, functioning during both acute and chronic inflammatory responses (65). Similarly, RANTES is also a chemotactic and pro-inflammatory cytokine with a wide variety of functions (66). Preliminary studies have also shown that RANTES may modulate the activity of MDSCs from the bone marrow and suppress cytotoxic T cell function (67). While chemotactic and pro-inflammatory cytokines may seem contrasting to elevated levels of immunosuppressive cells, heterotopic ossification and BMP-2 are known to result in increased inflammation (12,16). Chronic local inflammation may result in increased levels of pro-inflammatory cytokines while elevated levels of anti-inflammatory cells maintain a systemic immunosuppressive environment

that together adversely alter bone healing progression. This is further supported by work in the same bone nonunion model that shows elevated levels of inflammatory cytokines in non-healing rats versus healing rats (14). On the other hand, leptin was the cytokine most associated with the HMP groups. While leptin is largely known for its role in maintaining energy homeostasis, it has also been found to play a role in bone metabolism through a hypothalamic relay (69,70). Leptin-deficient mice exhibit decreased bone growth and bone formation rate as well as a decrease in osteoblasts (70). The association of leptin with the HMP groups could be a result of neuroendocrine function that is essential for the increased levels of bone formation observed. This is supported by work in the same bone nonunion model showing leptin to be the cytokine most associated with healing rats versus non-healing rats (14). Further studies investigating the role of the systemic immune response throughout the bone regeneration process are needed to more definitively understand the relationship between systemic immune mediators and local bone healing and to understand the role of immune dysregulation in nonunion progression.

Composite tissue polytrauma injuries present additional challenges for orthopedic surgeons with high rates of complications, such as nonunions, and long-term disability. Strategies that successfully heal injuries to bone alone may not adequately compensate for the additional loss of endogenous stem and progenitor cells from damaged vascularized muscle tissue, resulting in deficient healing and tissue regeneration. For example, in a pre-clinical composite bone-muscle defect model, five times the BMP-2 dosage (10ug) is required to achieve robust bone bridging compared to a bone only defect model (2ug) (14,28). Here, we found that despite addition of a volumetric muscle loss, 30ug BMP-2 delivered in the HMP system resulted in similar levels of bone regeneration and mechanical strength between the composite defect and bone defect only

chronic nonunion models. Based on this study, sustained delivery of moderately high doses of BMP-2 may be able to overcome more challenging bone healing scenarios, including chronic nonunions with concomitant muscle injury, and adverse immunological environments.

5. CONCLUSIONS

The results obtained in this study indicate that if appropriately delivered spatiotemporally, a high dose of BMP-2 may be able to overcome the additional challenges associated with chronic nonunions, including concomitant muscle injury and systemic immune dysregulation. Evaluation of the HMP delivery system showed improved bone regeneration and decreased side effects compared to the collagen sponge in clinically-relevant chronic nonunion models. Utilization of BMP-2 is an attractive option to address challenging musculoskeletal injuries because it has already received FDA approval and has shown success clinically. Further work will be essential to better understand biological mechanisms of nonunions, in particular how systemic and local immunological changes affect treatment outcomes.

ACKNOWLEDGEMENTS

This work was supported by funding from the Armed Forces Institute for Regenerative Medicine (AFIRM II) effort under award number W81XWH-14-2-0003. Opinions, interpretations, conclusions, and recommendations are those of the authors and are not necessarily endorsed by the Department of Defense. CEV acknowledges support by the National Science Foundation Graduate Research Fellowship under Grant No. DGE-1650044. Additionally, the authors wish to acknowledge the core facilities at the Parker H. Petit Institute for Bioengineering and Bioscience at the Georgia Institute of Technology for the use of their shared equipment, services, and

expertise. We also thank Ryan Akman, Ramesh Subbiah, Brennan Torstrick, Jason Wang, and Angela Lin for their assistance with surgeries and Levi Wood for usage of the MAGPIX multiplexing system.

REFERENCES

1. Schmidt-Bleek K, Marcucio R, Duda G. Future Treatment Strategies for Delayed Bone Healing. J Am Acad Orthop Surg. 2016;24(10):e134–5.
2. Pollack AN, Watkins-Castiollo SI. Fracture Trends [Internet]. The Burden of Musculoskeletal Diseases in the United States. 2014 [cited 2018 Dec 12]. Available from: http://www.boneandjointburden.org/
3. Harris AM, Althausen PL, Kellam J, Bosse MJ, Castillo R. Complications following limb-threatening lower extremity trauma. J Orthop Trauma. 2009 Jan;23(1):1–6.
4. Garcia P. Rodent non-union models. Eur Cells Mater. 2013;26:1–14.
5. Zura R, Xiong Z, Einhorn T, Watson JT, Ostrum RF, Prayson MJ, et al. Epidemiology of Fracture Nonunion in 18 Human Bones. JAMA Surg. 2016 Nov 16;151(11):e162775.
6. Low EE, Inkellis E, Morshed S. Complications and revision amputation following trauma-related lower limb loss. Injury. 2017 Feb 1;48(2):364–70.
7. MacKenzie EJ, Bosse MJ, Pollak AN, Webb LX, Swiontkowski MF, Kellam JF, et al. Long-Term Persistence of Disability Following Severe Lower-Limb Trauma<sbt aid="1025711">Results of a Seven-Year Follow-up</sbt> J Bone Jt Surg. 2005 Aug 1;87(8):1801.
8. Panteli M, Pountos I, Jones E, Giannoudis P V. Biological and molecular profile of fracture non-union tissue: Current insights. J Cell Mol Med. 2015 Apr 1;19(4):685–713.

9. Zura R, Della Rocca GJ, Mehta S, Harrison A, Brodie C, Jones J, et al. Treatment of chronic (>1 year) fracture nonunion: Heal rate in a cohort of 767 patients treated with low-intensity pulsed ultrasound (LIPUS). Injury. 2015 Oct 1;46(10):2036–41.

10. Vantucci CE, Roy K, Guldberg RE. Immunomodulatory strategies for immune dysregulation following severe musculoskeletal trauma. J Immunol Regen Med. 2018 Sep 1;2:21–35.

11. Hotchkiss RS, Monneret G, Payen D. Sepsis-induced immunosuppression: from cellular dysfunctions to immunotherapy. Nat Rev Immunol. 2013;13(12):862–74.

12. Casey E. Vantucci, Hyunhee Ahn MLS, Pradhan P, , Levi B. Wood, Guldberg RE, Roy K, Willett NJ. Development of Systemic Immune Dysregulation in a Rat Trauma Model with Biomaterial-Associated Infection. bioRxiv. 2020 Jan 11;1–36.

13. Flohe S, Flohe SB, Schade FU, Waydhas C. Immune response of severely injured patients - Influence of surgical intervention and therapeutic impact. Langenbeck's Arch Surg. 2007;392(5):639–48.

14. Cheng A, Krishnan L, Pradhan P, Weinstock LD, Wood LB, Roy K, et al. Impaired bone healing following treatment of established nonunion correlates with serum cytokine expression. J Orthop Res. 2018 Nov 27;

15. Walsh MC, Takegahara N, Kim H, Choi Y. Updating osteoimmunology: regulation of bone cells by innate and adaptive immunity. Nat Rev Rheumatol. 2018 Mar 11;14(3):146–56.

16. Kolambkar YM, Boerckel JD, Dupont KM, Bajin M, Huebsch N, Mooney DJ, et al. Spatiotemporal delivery of bone morphogenetic protein enhances functional repair of segmental bone defects. Bone. 2011;49(3):485–92.

17. Krishnan L, Priddy LB, Esancy C, Klosterhoff BS, Stevens HY, Tran L, et al. Delivery vehicle effects on bone regeneration and heterotopic ossification induced by high dose BMP-2. Acta Biomater. 2017;49:101–12.

18. Krishnan L, Priddy LB, Esancy C, Li M-TA, Stevens HY, Jiang X, et al. Hydrogel-based Delivery of rhBMP-2 Improves Healing of Large Bone Defects Compared With Autograft. Clin Orthop Relat Res. 2015 Sep 28;473(9):2885–97.

19. Lykissas M, Gkiatas I. Use of recombinant human bone morphogenetic protein-2 in spine surgery. World J Orthop. 2017 Jul 18;8(7):531–5.

20. Conway JD, Shabtai L, Bauernschub A, Specht SC. BMP-7 Versus BMP-2 for the Treatment of Long Bone Nonunion. Orthopedics. 2014 Dec 1;37(12):e1049–57.

21. Wei F, Zhou Y, Wang J, Liu C, Xiao Y. The Immunomodulatory Role of BMP-2 on Macrophages to Accelerate Osteogenesis. Tissue Eng Part A. 2018 Apr 1;24(7–8):584–94.

22. Boerckel JD, Kolambkar YM, Dupont KM, Uhrig BA, Phelps EA, Stevens HY, et al. Effects of protein dose and delivery system on BMP-mediated bone regeneration. Biomaterials. 2011 Aug;32(22):5241–51.

23. Uludag H, Gao T, Porter TJ, Friess W, Wozney JM. Delivery systems for BMPs: factors contributing to protein retention at an application site. J Bone Joint Surg Am. 2001;83–A Suppl 1(Pt 2):S128-35.

24. Tannoury CA, An HS. Complications with the use of bone morphogenetic protein 2 (BMP-2) in spine surgery. Spine J. 2014;14(3):552–9.

25. Shields LBE, Raque GH, Glassman SD, Campbell M, Vitaz T, Harpring J, et al. Adverse Effects Associated With High-Dose Recombinant Human Bone Morphogenetic Protein-2 Use in Anterior Cervical Spine Fusion. Spine (Phila Pa 1976). 2006 Mar 1;31(5):542–7.

26. Lee K-B, Taghavi CE, Song K-J, Sintuu C, Yoo JH, Keorochana G, et al. Inflammatory Characteristics of rhBMP-2 In Vitro and in an In Vivo Rodent Model. Spine (Phila Pa 1976). 2011 Feb 1;36(3):E149–54.

27. Zara JN, Siu RK, Zhang X, Shen J, Ngo R, Lee M, et al. High doses of bone morphogenetic protein 2 induce structurally abnormal bone and inflammation in vivo. Tissue Eng Part A. 2011 May;17(9–10):1389–99.

28. Ruehle MA, Krishnan L, Vantucci CE, Wang Y, Stevens HY, Roy K, et al. Effects of BMP-2 dose and delivery of microvascular fragments on healing of bone defects with concomitant volumetric muscle loss. J Orthop Res. 2019 Jan 16;

29. Cowan CM, Aghaloo T, Chou Y-F, Walder B, Zhang X, Soo C, et al. MicroCT Evaluation of Three-Dimensional Mineralization in Response to BMP-2 Doses *In Vitro* and in Critical Sized Rat Calvarial Defects. Tissue Eng. 2007 Mar;13(3):501–12.

30. Sandhu HS, Kanim LE, Kabo JM, Toth JM, Zeegen EN, Liu D, et al. Effective doses of recombinant human bone morphogenetic protein-2 in experimental spinal fusion. Spine (Phila Pa 1976). 1996 Sep 15;21(18):2115–22.

31. Kolambkar YM, Dupont KM, Boerckel JD, Huebsch N, Mooney DJ, Hutmacher DW, et al. An alginate-based hybrid system for growth factor delivery in the functional repair of large bone defects. Biomaterials. 2011;32(1):65–74.

32. Agrawal V, Sinha M. A review on carrier systems for bone morphogenetic protein-2. J Biomed Mater Res Part B Appl Biomater. 2017 May 1;105(4):904–25.

33. Begam H, Nandi SK, Kundu B, Chanda A. Strategies for delivering bone morphogenetic protein for bone healing. Mater Sci Eng C. 2017 Jan 1;70:856–69.

34. Agarwal R, García AJ. Biomaterial strategies for engineering implants for enhanced

osseointegration and bone repair. Adv Drug Deliv Rev. 2015 Nov 1;94:53–62.

35. Pakulska MM, Miersch S, Shoichet MS. Designer protein delivery: From natural to engineered affinity-controlled release systems. Science (80-). 2016 Mar 18;351(6279):aac4750-aac4750.

36. Miller T, Goude MC, McDevitt TC, Temenoff JS. Molecular engineering of glycosaminoglycan chemistry for biomolecule delivery. Acta Biomater. 2014 Apr;10(4):1705–19.

37. Hettiaratchi MH, Rouse T, Chou C, Krishnan L, Stevens HY, Li M-TA, et al. Enhanced in vivo retention of low dose BMP-2 via heparin microparticle delivery does not accelerate bone healing in a critically sized femoral defect. Acta Biomater. 2017 Sep 1;59:21–32.

38. Hettiaratchi MH, Miller T, Temenoff JS, Guldberg RE, McDevitt TC. Heparin microparticle effects on presentation and bioactivity of bone morphogenetic protein-2. Biomaterials. 2014;35(25):7228–38.

39. Hettiaratchi MH, Krishnan L, Rouse T, Chou C, McDevitt TC, Guldberg RE. Heparin-mediated delivery of bone morphogenetic protein-2 improves spatial localization of bone regeneration. Sci Adv. 2020 Jan 3;6(1):eaay1240.

40. Oest ME, Dupont KM, Kong H-J, Mooney DJ, Guldberg RE. Quantitative assessment of scaffold and growth factor-mediated repair of critically sized bone defects. J Orthop Res. 2007 Jul;25(7):941–50.

41. Willett NJ, Li M-TA, Uhrig BA, Boerckel JD, Huebsch N, Lundgren TS, et al. Attenuated Human Bone Morphogenetic Protein-2–Mediated Bone Regeneration in a Rat Model of Composite Bone and Muscle Injury. Tissue Eng Part C Methods. 2013;19(4):316–25.

42. Bouxsein ML, Boyd SK, Christiansen BA, Guldberg RE, Jepsen KJ, Müller R. Guidelines

for assessment of bone microstructure in rodents using micro-computed tomography. J Bone Miner Res. 2010 Jun 7;25(7):1468–86.

43. Boerckel JD, Kolambkar YM, Stevens HY, Lin ASP, Dupont KM, Guldberg RE. Effects of in vivo mechanical loading on large bone defect regeneration. J Orthop Res. 2012;30(7):1067–75.

44. Hawkins RB, Raymond SL, Stortz JA, Horiguchi H, Brakenridge SC, Gardner A, et al. Chronic Critical Illness and the Persistent Inflammation, Immunosuppression, and Catabolism Syndrome. Front Immunol. 2018 Jul 2;9.

45. Nicola R. Early Total Care versus Damage Control: Current Concepts in the Orthopedic Care of Polytrauma Patients. ISRN Orthop. 2013 Mar 21;2013:329452.

46. Tschoeke SK, Ertel W. Immunoparalysis after multiple trauma. Injury. 2007;38(12):1346–57.

47. Kimura F, Shimizu H, Yoshidome H, Ohtsuka M, Miyazaki M. Immunosuppression following surgical and traumatic injury. Surg Today. 2010;40(9):793–808.

48. Flohe SB, Flohe S, Schade FU. Deterioration of the immune system after trauma: signals and cellular mechanisms. Innate Immun. 2008;

49. Stahel PF, Smith WR, Moore EE. Role of biological modifiers regulating the immune response after trauma. Injury. 2007;38(12):1409–22.

50. Desai KH, Tan CS, Leek JT, Maier R V, Tompkins RG, Storey JD. Dissecting inflammatory complications in critically injured patients by within-patient gene expression changes: A longitudinal clinical genomics study. PLoS Med. 2011;8(9).

51. Gentile LF, Cuenca AG, Efron P a, Ang D. Persistent inflammation and immunosuppression: A common syndrome and new horizon for surgical intensive care. J

Trauma Acute Care Surg. 2012;72(6):1491–501.

52. Vanzant EL, Lopez CM, Ozrazgat-Baslanti T, Ungaro R, Davis R, Cuenca AG, et al. Persistent Inflammation, Immunosuppression and Catabolism Syndrome after Severe Blunt Trauma. J Trauma Acute Care Surg. 2014;76(1):21–30.

53. Sengupta P. The Laboratory Rat: Relating Its Age With Human's. Int J Prev Med. 2013 Jun;4(6):624–30.

54. Fulop T, Larbi A, Dupuis G, Le Page A, Frost EH, Cohen AA, et al. Immunosenescence and Inflamm-Aging As Two Sides of the Same Coin: Friends or Foes? Front Immunol. 2018 Jan 10;8:1960.

55. Ventura MT, Casciaro M, Gangemi S, Buquicchio R. Immunosenescence in aging: between immune cells depletion and cytokines up-regulation. Clin Mol Allergy. 2017;15:21.

56. Hettiaratchi M, Krishnan L, Li M-TA, Temenoff J. BMP-2-Loaded Heparin Microparticles Facilitate Functional Bone Formation in Large Bone Defects | Request PDF. In: Tissue Engineering and Regenerative Medicine International Society World Congress. Boston; 2015.

57. Capila I, Linhardt RJ. Heparin-Protein Interactions. Angew Chemie Int Ed. 2002 Feb 1;41(3):390–412.

58. Deepa SS, Umehara Y, Higashiyama S, Itoh N, Sugahara K. Specific Molecular Interactions of Oversulfated Chondroitin Sulfate E with Various Heparin-binding Growth Factors. J Biol Chem. 2002 Nov 15;277(46):43707–16.

59. Gandhi NS, Mancera RL. Prediction of heparin binding sites in bone morphogenetic proteins (BMPs). Biochim Biophys Acta - Proteins Proteomics. 2012 Dec;1824(12):1374–

81.

60. Damon DH, Lobb RR, D'Amore PA, Wagner JA. Heparin potentiates the action of acidic fibroblast growth factor by prolonging its biological half-life. J Cell Physiol. 1989 Feb;138(2):221–6.

61. Shen X, Fang J, Lv X, Pei Z, Wang Y, Jiang S, et al. Heparin impairs angiogenesis through inhibition of microRNA-10b. J Biol Chem. 2011 Jul 29;286(30):26616–27.

62. Anderson SE, Han WM, Srinivasa V, Mohiuddin M, Ruehle MA, Moon JY, et al. Determination of a critical size threshold for volumetric muscle loss in the mouse quadriceps. Tissue Eng - Part C Methods. 2019 Feb 1;25(2):59–70.

63. Suchacki KJ, Cawthorn WP. Molecular Interaction of Bone Marrow Adipose Tissue with Energy Metabolism. Curr Mol Biol Reports. 2018 Jun 28;4(2):41–9.

64. Ozaki K, Leonard WJ. Cytokine and cytokine receptor pleiotropy and redundancy. J Biol Chem. 2002 Aug 16;277(33):29355–8.

65. Wang L-Y, Tu Y-F, Lin Y-C, Huang C-C. CXCL5 signaling is a shared pathway of neuroinflammation and blood–brain barrier injury contributing to white matter injury in the immature brain. J Neuroinflammation. 2016 Dec 6;13(1):6.

66. Conti P, DiGioacchino M. MCP-1 and RANTES Are Mediators of Acute and Chronic Inflammation. Allergy Asthma Proc. 2001 May 1;22(3):133–7.

67. Yao M, Brummer G, Acevedo D, Cheng N. Cytokine Regulation of Metastasis and Tumorigenicity. Adv Cancer Res. 2016 Jan 1;132:265–367.

68. Chen D, Zhao M, Mundy GR. Bone morphogenetic proteins. Growth Factors. 2004;22(4):233–41.

69. Turner RT, Kalra SP, Wong CP, Philbrick KA, Lindenmaier LB, Boghossian S, et al.

Peripheral leptin regulates bone formation. J Bone Miner Res. 2013 Jan;28(1):22–34.

70. Upadhyay J, Farr OM, Mantzoros CS. The role of leptin in regulating bone metabolism. Metabolism. 2015 Jan;64(1):105–13.

FIGURES AND FIGURE LEGENDS

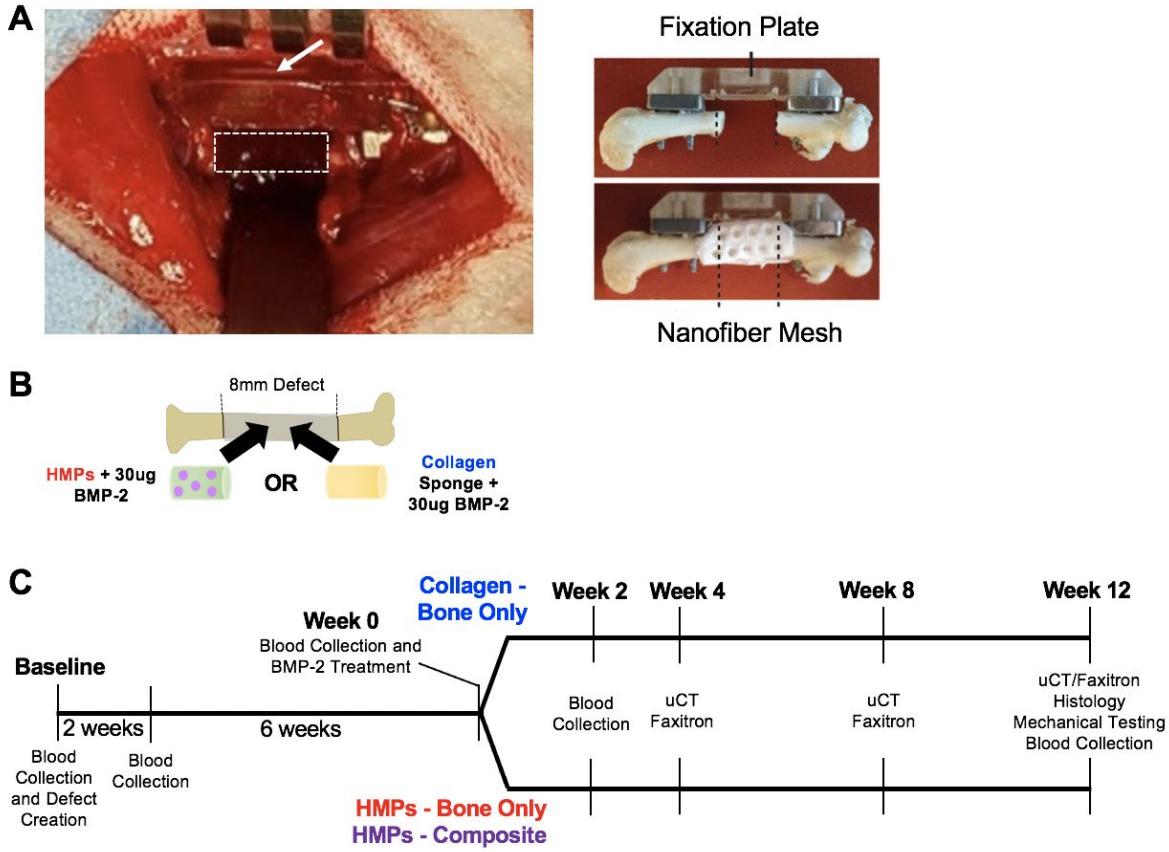

Figure 1. *Clinically-relevant bone nonunion models.* A) Each animal received an 8mm femoral segmental defect, stabilized by a polysulfone internal fixation plate. The white, dotted rectangle indicates the location of the defect and the white arrow indicates the fixation plate. Additionally, one group of animals will also receive an 8mm volumetric muscle loss in the adjacent quadricep muscle (not shown). Ex vivo imaging shows the fixation plate stabilizing the femur and the nanofiber mesh construct within the defect site, which is used for the HMP hybrid delivery system. Ex vivo images are reproduced with permission from Krishnan et al (18). B) The defects will be treated with 30ug BMP-2 delivered in HMPs within an alginate/nanofiber mesh construct or 30ug BMP-2 delivered on an adsorbable collagen sponge. C) The timeline of the study indicates the timepoints for defect creation, BMP-2 treatment, blood collections, uCT scans, radiographic images (Faxitron), histology, and mechanical testing.

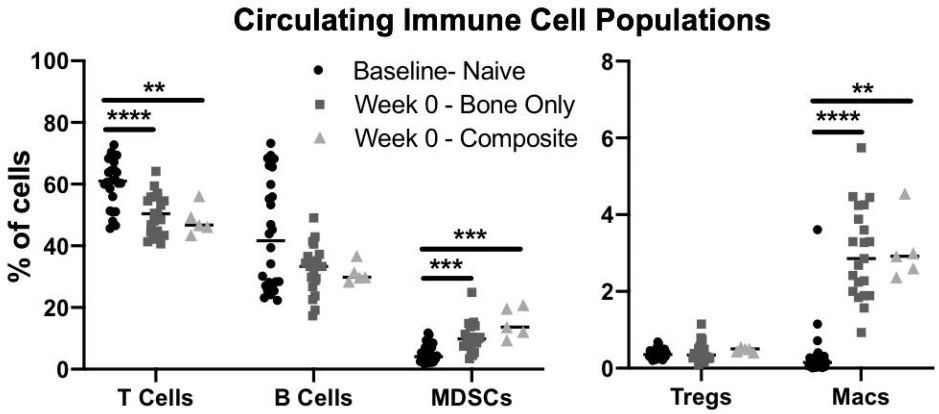

Figure 2. *Circulating Immune Cell Populations.* Circulating immune cell populations at baseline prior to defect creation, and at Week 0 prior to BMP-2 treatment (8 weeks post-defect creation) for the bone only defect group and the composite defect group. Significance was determined using one-way ANOVA with $p<0.01$ (**), $p<0.005$ (***), and $p<0.001$ (****).

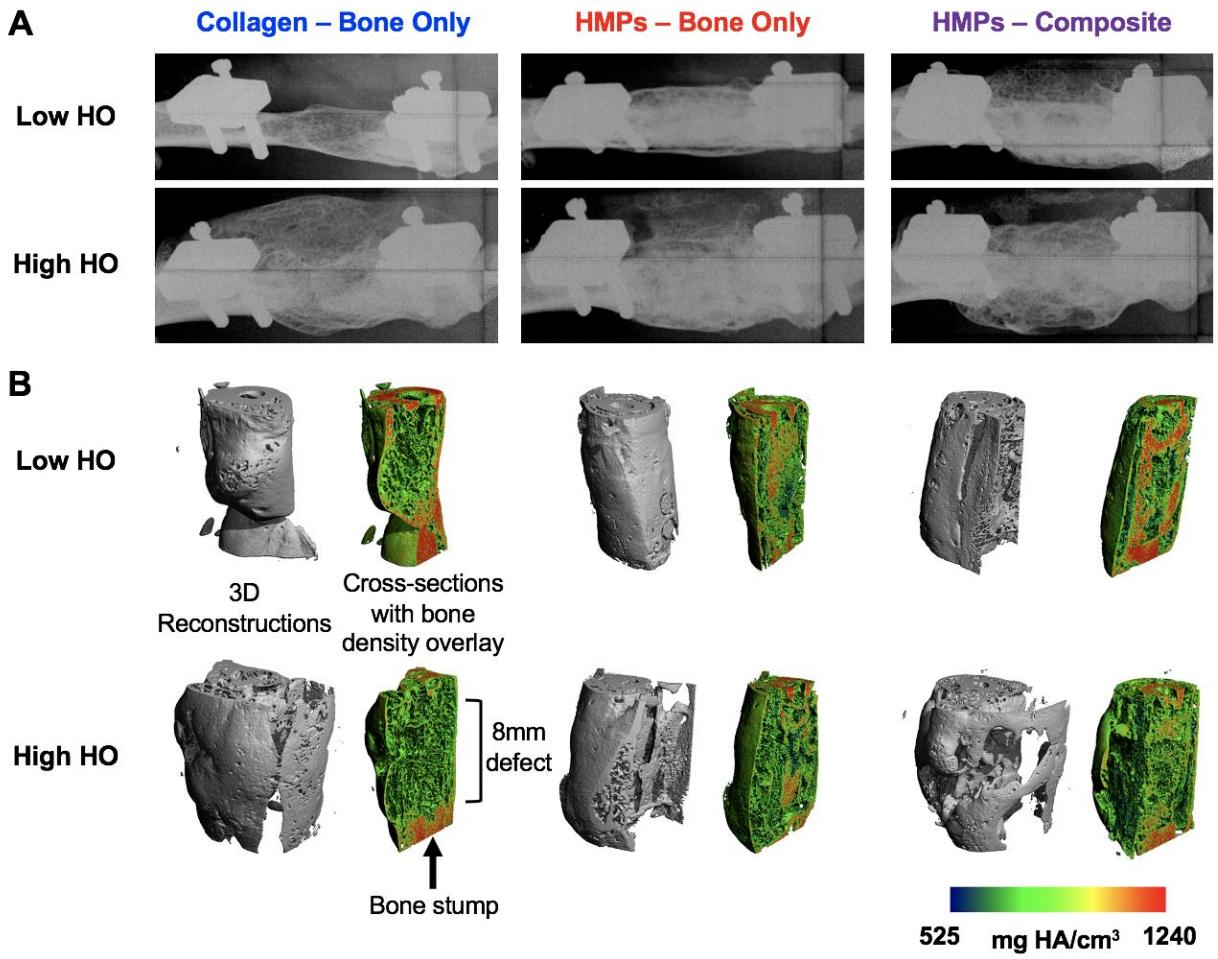

Figure 3. *Endpoint radiographs and uCT reconstructions of regenerating bone defects.* A) Week 12 endpoint (20 weeks post-injury) representative radiograph images of both low heterotopic ossification (HO) and high HO for each group are shown. B) uCT reconstructions with both the 3D reconstruction and the cross section with the bone density overlay are shown.

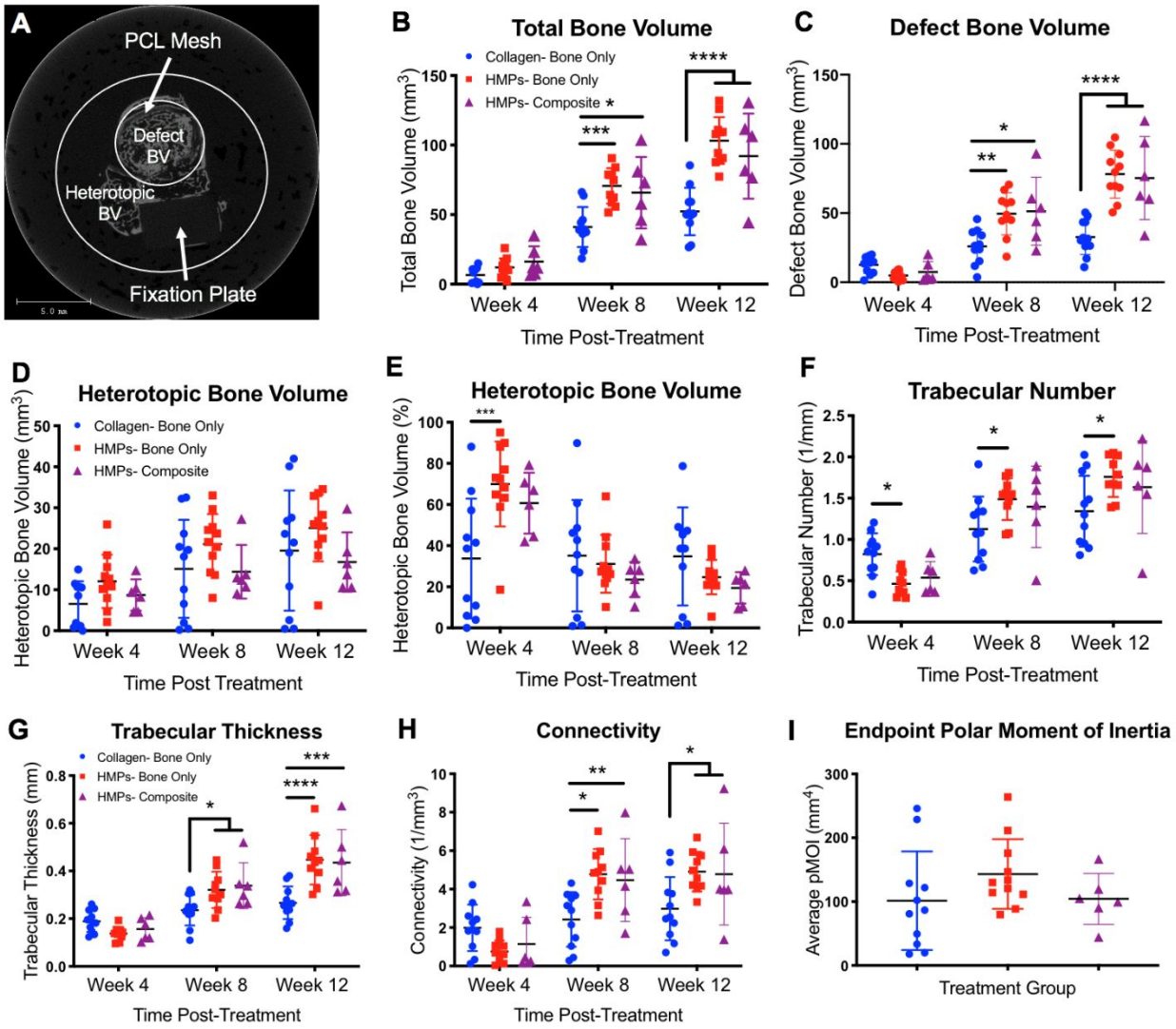

Figure 4. *Longitudinal evaluation of bone regeneration and morphological bone characteristics.* A) A representative image of one slice taken from uCT imaging shows the defect bone volume region and the heterotopic bone volume region. In addition, the shadow of the fixation plate can be seen, and the PCL mesh can be seen just inside the defect bone volume region. Total bone volume includes both defect bone volume and heterotopic bone volume. Longitudinal quantification of total bone volume (B), defect bone volume (C), absolute heterotopic bone volume (D), and percent of heterotopic bone (E) reveals differences in bone regeneration over time between the collagen and HMP groups. Morphological bone characteristics, including trabecular number (F), trabecular thickness (G), and connectivity (H), were also evaluated and

reveal differences in bone structure over time between the collagen and HMP groups. There were no differences in the polar moment of inertia between groups (I). Significance was determined using two-way ANOVA with Sidak's multiple comparisons test where $p<0.05$ (*), $p<0.01$ (**), $p<0.005$ (***), and $p<0.001$ (****).

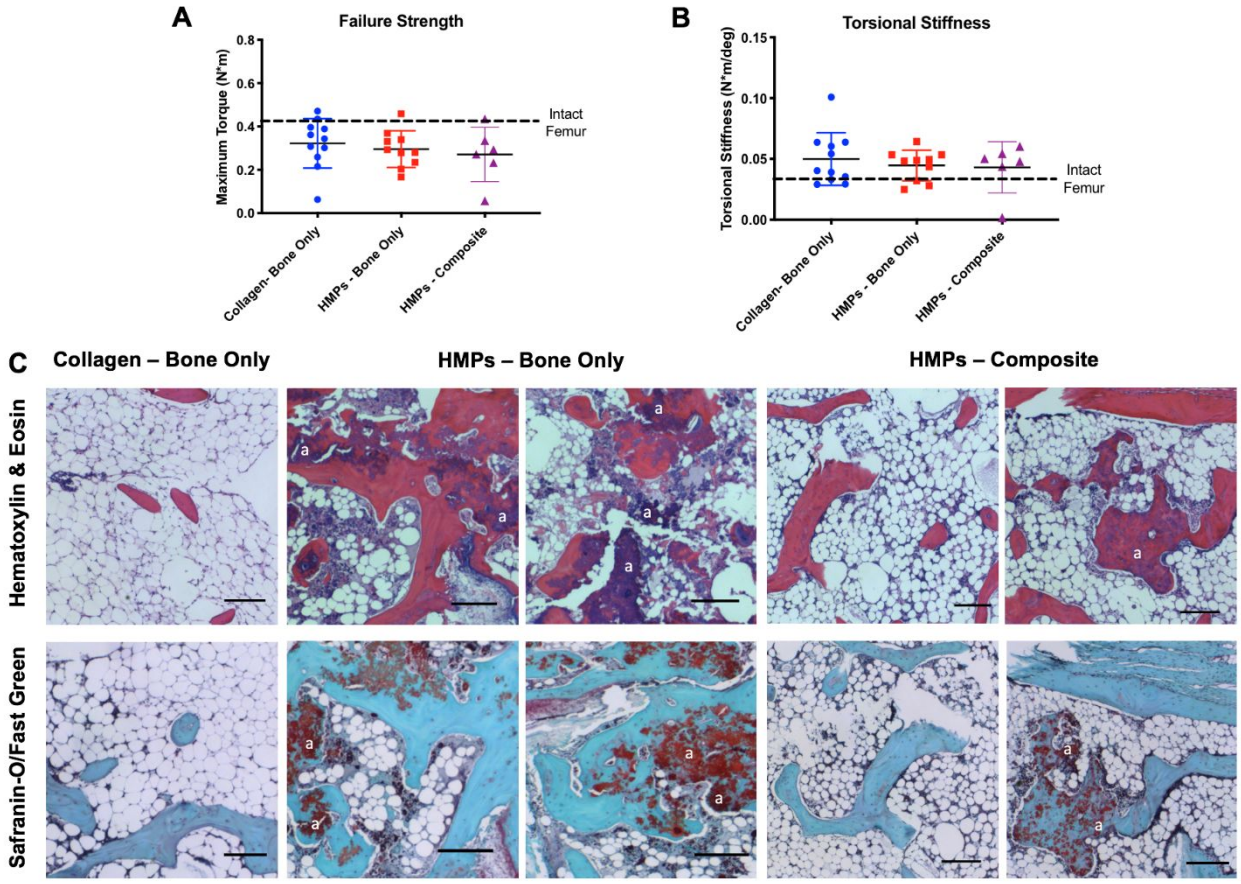

Figure 5. *Biomechanical testing and histological analysis.* Mechanical testing of A) failure strength and B) torsional stiffness shows no difference between groups. The dotted black line indicates the average failure strength and torsional stiffness of the contralateral intact femurs, respectively. C) Staining with Hematoxylin & Eosin and Safranin-O/Fast Green at the 12 week endpoint (20 weeks post-injury) shows mineralized tissue in the HMP groups and non-mineralized, marrow-like tissue in the collagen group. Residual alginate can also be seen in the HMP groups and examples are marked with an "a". Scale – 150um.

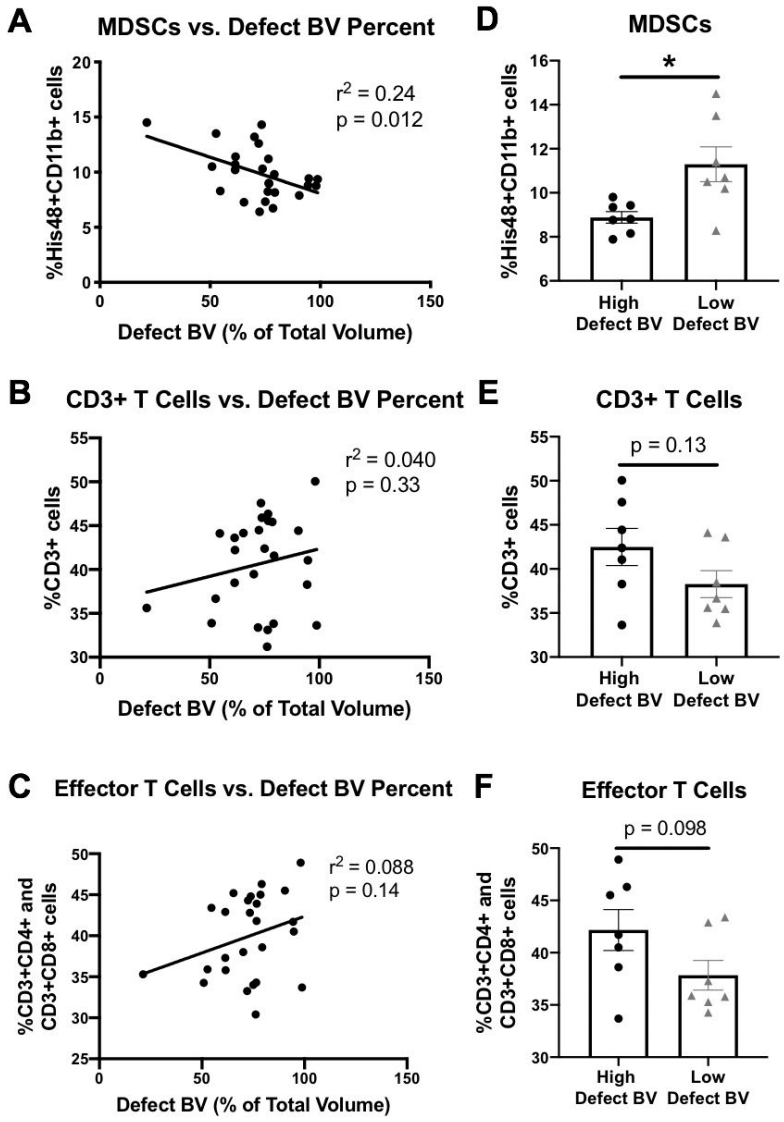

Figure 6. *Linear regression analyses comparing systemic immune cell populations with defect bone volume percent.* Linear regressions comparing defect bone volume as a percent of total bone volume versus week 12 (endpoint) circulating immune cell populations for A) MDSCs, B) CD3+ T cells, and C) effector T cells which includes both helper (CD3+CD4+) and cytotoxic (CD3+CD8+) T cells with r^2 and p values as indicated. Removal of the middle 50% of the data set according to defect bone volume percent left 25% of the lowest defect bone volume percent samples and 25% of the highest defect bone volume percent samples. The high defect bone volume percent samples and the low defect bone volume percent samples were then compared

for their levels of D) MDSCs, E) CD3+ T cells, and F) effector T cells. Mann-Whitney or Student's t-test were performed with p values as indicated or a * (p = 0.011).

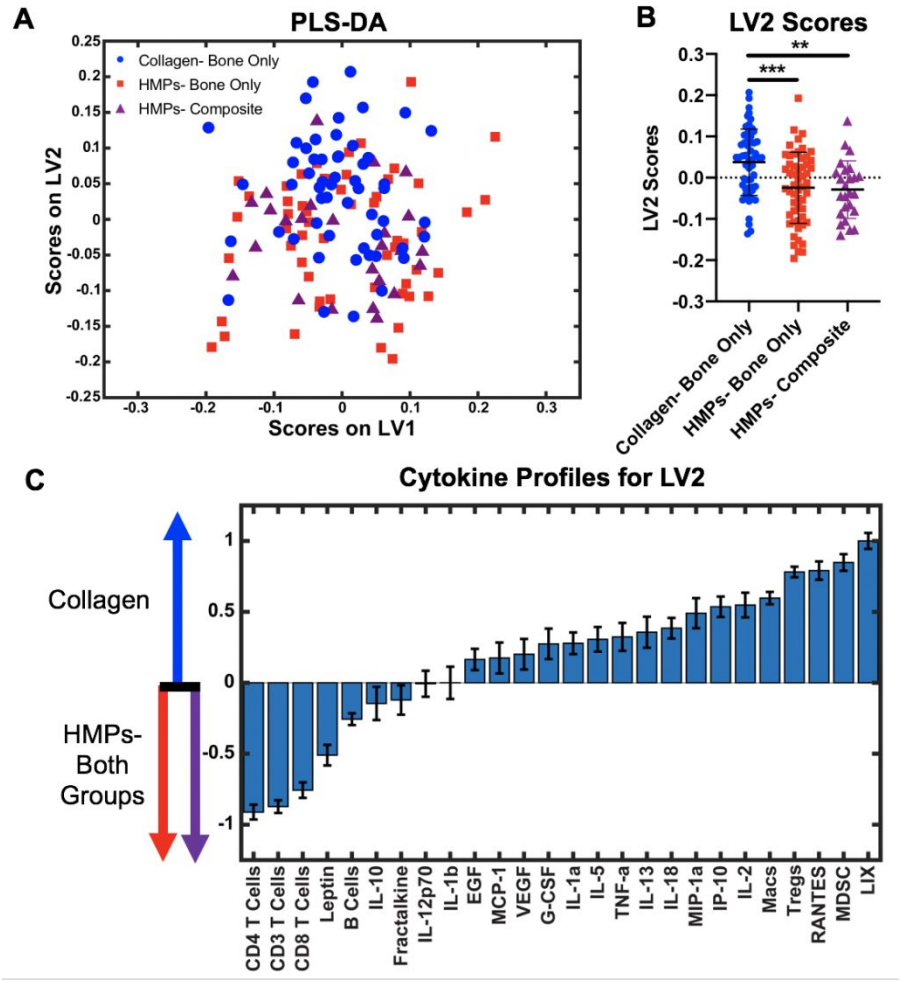

Figure 7. *Multivariate analysis of the systemic immune response.* A) PLS-DA plot shows all cytokine levels and cell populations for the collagen treated group (blue circles), the HMP treated bone only nonunion model (red squares), and the HMP treated composite defect nonunion model (purple triangles) plotted on the latent variable 1 (LV1) axis and the latent variable 2 (LV2) axis. Cytokine levels and cell populations were pooled across all time points. Significance was determined using one-way ANOVA with Tukey's post hoc test where $p<0.01$(**) and $p<0.005$(***). B) Plotting only LV2 scores reveals a significant separation

between the collagen group and the HMP groups. C) The LV2 loading plot shows the top factors most correlated with positive LV2 scores on the right (collagen group) and the top factors most correlated with negative LV2 scores on the left (HMP groups). There was no significant separation between the two HMP treated groups.

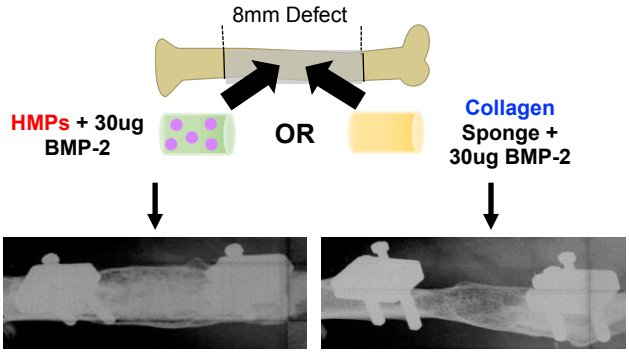
8mm Defect
HMPs + 30ug BMP-2
OR
Collagen Sponge + 30ug BMP-2